VIP Li-Ion Batteries Very Important Paper

DOI: 10.1002/anie.201406135

Sustainable Electrical Energy Storage through the Ferrocene/Ferrocenium Redox Reaction in Aprotic Electrolyte**

*Yu Zhao, Yu Ding, Jie Song, Gang Li, Guangbin Dong, John B. Goodenough, and Guihua Yu**

Abstract: *The large-scale, cost-effective storage of electrical energy obtained from the growing deployment of wind and solar power is critically needed for the integration into the grid of these renewable energy sources. Rechargeable batteries having a redox-flow cathode represent a viable solution for either a Li-ion or a Na-ion battery provided a suitable low-cost redox molecule soluble in an aprotic electrolyte can be identified that is stable for repeated cycling and does not cross the separator membrane to the anode. Here we demonstrate an environmentally friendly, low-cost ferrocene/ferrocenium molecular redox couple that shows about 95% energy efficiency and about 90% capacity retention after 250 full charge/discharge cycles.*

The rapidly expanding deployment of renewable energy sources, which supply electric power from wind and solar energy to a grid servicing a variable and increasing energy demand, requires the development of distributed electrical energy storage that may be either portable or stationary.[1,2] Rechargeable batteries offer such an electrical energy storage, but all of the targets of cost, safety, service life, and energy and power density in a single existing rechargeable battery have yet to be met. Recently, rechargeable batteries with a solid oxide Li-ion electrolyte separating an aprotic anolyte and an aqueous flow-through catholyte have been explored.[3–7] These batteries would offer a water soluble redox molecule and a metallic lithium anode, but a suitable solid Li^+-electrolyte separator has yet to be developed. This cell configuration is potentially advantageous owing to the low cost of aqueous electrolytes and the extremely high capacity of a lithium anode. However, to avoid water decomposition, the H_2/O_2 evolution potential limits the applicable potential change of such cells. More importantly, the solid Li^+-electrolyte separator must be sufficiently robust mechanically to be fabricated as a thin large-area membrane and have chemical stability in a corrosive aqueous catholyte to prevent the lithium anode from getting into contact with the aqueous catholyte.[8]

Alternatively, semipermeable, mechanically robust, and flexible separators have been developed that block dendrites from an alkali-metal anode.[9] They allow a flow-through catholyte containing an aprotic liquid with a large voltage window, for example, formamide and amides,[10,11] provided the redox molecule of the catholyte is soluble in the liquid electrolyte and is blocked from crossing the membrane into the anode. A liquid flow-through cathode offers a fundamentally different, higher capacity and rate capability than a solid insertion-compound cathode and the use of an aprotic liquid electrolyte permits a broader potential window than is possible with a conventional aqueous flow-through battery. Herein, we explore the use of inexpensive ferrocene dissolved in dimethylformamide as the liquid cathode of a 3.6 V Li-ion cell with a solid Li^+-electrolyte separator (see the Supporting Information, SI, for more details). The liquid cathode exhibits a high-rate discharging capability with high energy efficiency and stable discharge potential, which are comparable to those of Li-ion batteries and superior to the conventional redox-flow batteries based on proton chemistry.

In ferrocene, two cyclopentadienyl ligands, C_5H_5, lie on top of each other with the Fe atom sandwiched in the middle. The π orbitals of the C_5H_5 rings and the Fe d orbitals are responsible for coordination and chemical reactivity.[12] In the ground state, the frontier orbital of ferrocene (Figure 1a) is generally accepted as being $(e_{2g})^4(a_{1g})^2$, whereas for ferrocenium the orbital structure is generally accepted as being $(e_{2g})^4(a_{1g})^1$.[13] The activation energy required for the orbital electronic structure conversion is as low as approximately 10 kJ mol^{-1} in most organic solvents[14] with a rate constant[15] that is much greater than that of other redox couples used in conventional redox-flow batteries.[16] Besides, good thermal stability, the high solubility in most organic solvents,[17] and a redox potential of 3.6 V vs. Li^+/Li make ferrocene an attractive material for the construction of a liquid cathode Li-ion battery.

The working principle of such a battery is based on the reversible redox reaction between ferrocene and ferrocenium (Figure 1b). Upon charging, Li-ions move from the cathode to the anode through a NASICON-type $Li_{1+x+3z}Al_x(Ti,Ge)_{2-x}Si_{3z}P_{3-z}O_{12}$ (LATP) membrane in which the Li-ion diffuses through a vacancy diffusion mechanism,[18,19] while electrons move from the cathode to the anode through an external circuit. During charging, ferrocene is oxidized into ferrocenium in the cathode, while a Li-ion is reduced to Li in the

[*] Dr. Y. Zhao,[+] Y. Ding,[+] Dr. J. Song, Prof. J. B. Goodenough, Prof. G. Yu
Materials Science and Engineering Program and Department of Mechanical Engineering, The University of Texas at Austin
Austin, TX 78712 (USA)
E-mail: ghyu@austin.utexas.edu
Dr. G. Li, Prof. G. Dong
Department of Chemistry, The University of Texas at Austin
Austin, TX 78712 (USA)

[+] These authors contributed equally to this work.

[**] G.Y. acknowledges the financial support of the faculty start-up grant from the University of Texas at Austin and The Welch Foundation grant (F 1861). J.B.G. acknowledges the support by the Robert A. Welch Foundation of Houston, Texas. G.D. acknowledges the Welch Foundation grant (F 1781).

Supporting information for this article is available on the WWW under http://dx.doi.org/10.1002/anie.201406135.

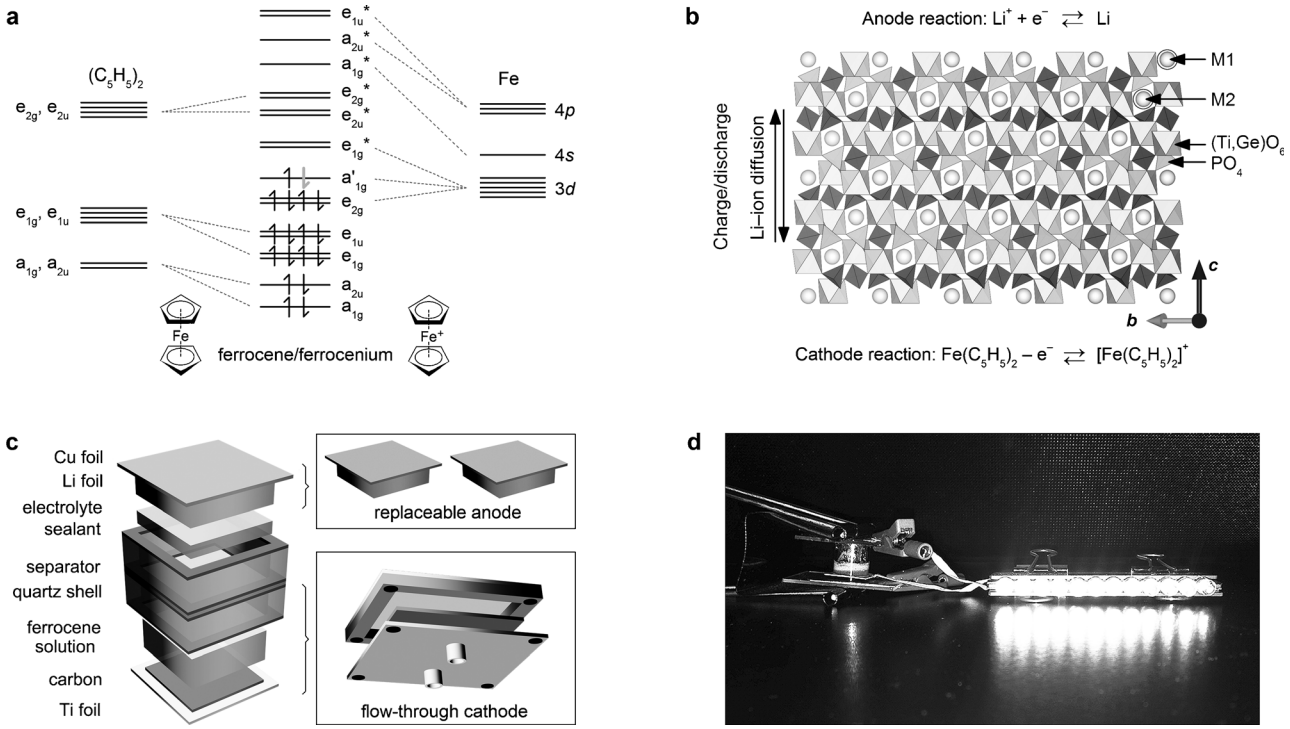

Figure 1. Rationality of using the ferrocene/ferrocenium redox couple to design an alkali-ion battery. a) The frontier orbital electronic structure of ferrocene/ferrocenium. b) Working principle of the cell. A NASICON-type $Li_{1+x+3z}Al_x(Ti,Ge)_{2-x}Si_{3z}P_{3-z}O_{12}$ membrane is used as separator, which only allows Li-ions to pass through. In the NASICON structure, Li-ions occupy two positions in the conduction channels: the M1 site, which is coordinated by a trigonal antiprism of oxygen atoms, and the M2 site, which has a distorted eightfold coordination. Long-range ion conduction in the NASICON structure is built up by ion diffusion between the M1 and M2 sites. $(Ti,Ge)O_6$ octahedrons and PO_4 tetrahedrons in the NASICON-type structure are shown in green and purple, respectively. c) Proposed cell design and configuration. The cathode part is composed of a Ti foil as the supporting substrate, activated carbon as the current collector, and ferrocene solution as liquid cathode. A NASICON-type $Li_{1+x+3z}Al_x(Ti,Ge)_{2-x}Si_{3z}P_{3-z}O_{12}$ membrane is used to separate the cathode from the anode. The cell was sealed with the Surlyn resin. d) An experimental demonstration of the power performance of the cell showing a power output high enough to light twelve LED bulbs simultaneously. The solid electrolyte is 0.64 cm^2 in area.

anode. Correspondingly, discharging is the reverse process relative to charging. The cell structure design is flexible following the basic rule that the cathode and anode should be isolated by a Li-ion-conducting ceramic membrane. In this study, a home-built cell (Figure 1c) composed of a cathode compartment (Ti foil as supporting substrate, activated carbon as current collector, and ferrocene dissolved in selected organic solvent as liquid cathode), a LATP separator (electrochemically stable at a potential range between 2.8–6 V vs. Li^+/Li),[3,6] and an anode compartment (conventional organic electrolyte or polymer electrolyte as buffer layer, Li@Cu foil as anode) is used. Combining the concept and advantages of Li-ion batteries and redox-flow batteries, the cell can be designed with a flow-through cathode[20,21] and a replaceable anode, both of which can be independently scalable. The benefit from such a configuration relies in the reduced size of individual cells to further lower the cost of the whole battery pack. The high power output of a fully charged cell was impressively demonstrated by simultaneously lighting twelve white LED bulbs (Figure 1d).

The solvent might interact with either ferrocene or ferrocenium, leading to a significant solvent dependence of the redox potential. Therefore, the redox behavior of ferrocene/ferrocenium in some representative inexpensive solvents such as *N*,*N*-dimethylformamide (DMF), *N*,*N*-dimetylacetamide (DMA) and tetrahydrofuran (THF) were tested. The commercial organic electrolyte for Li-ion batteries, ethylene carbonate (EC)/diethyl carbonate (DEC), was also tested as reference. The dQ/dV plots (Figure 2a) of 0.1 M ferrocene in these solvents in the presence of 1 M $LiPF_6$ exhibit quite different redox behavior at the same current density: DMA showed the highest redox potential followed by DMF and THF with EC/DEC being the lowest. However, the reversible capacity of ferrocene achieved in DMA was the smallest among the solvents tested. The redox potential depends on the interactions between ferrocene/ferrocenium and solvent molecules through possible interactions between the hydrogen-bonding acid and base moieties of the solvent and the members of the ferrocene/ferrocenium couple.[22] It's found in our studies that DMF was the most suitable solvent for the ferrocene/ferrocenium redox reaction considering the smaller overpotential (~70 mV) and higher reduction potential (~3.6 V vs. Li^+/Li) of ferrocenium. Moreover, cyclic voltammetry (CV) measurements with a low sweeping rate (Figure 2b) confirmed that the redox reaction of ferrocene/ferrocenium was reversible as the cathodic and anodic peaks were symmetric, and this redox reaction was the sole reaction taking place in DMF, suggesting the stability of both

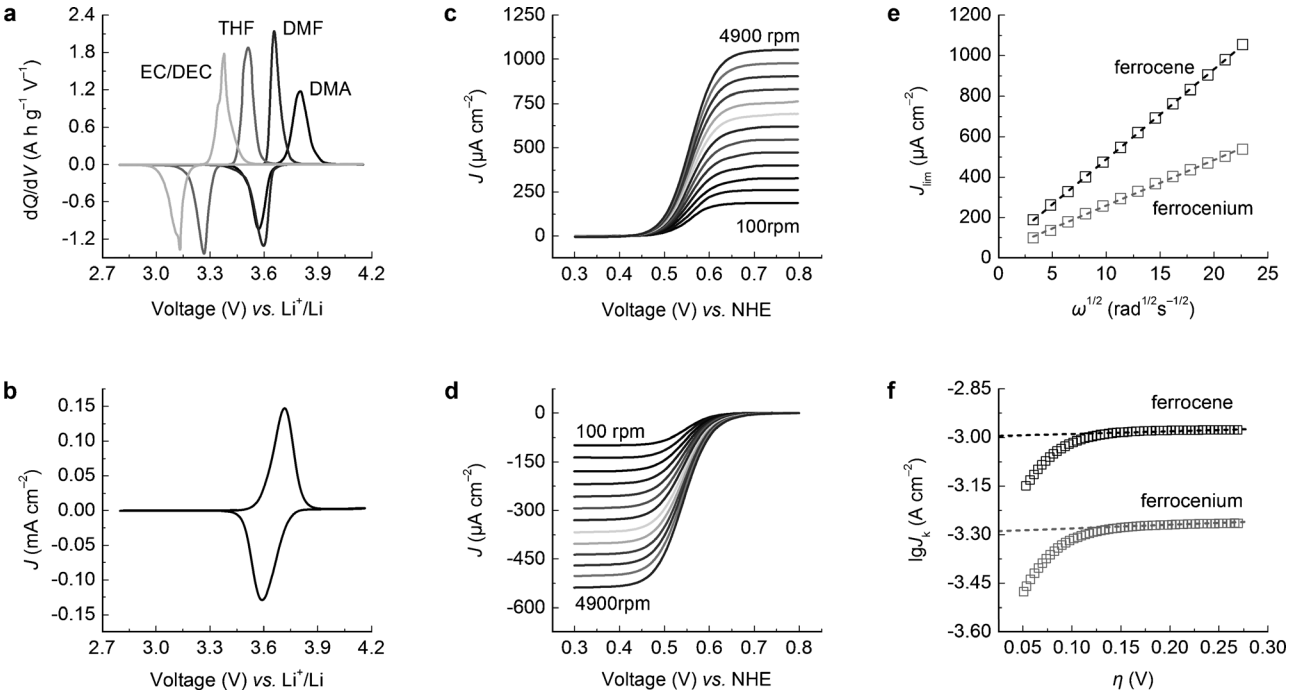

Figure 2. The redox behavior of the ferrocene/ferrocenium couple in an aprotic solvent. a) Solvent-dependent redox potential of ferrocene/ferrocenium in DMA, DMF, THF, and EC/DEC solvents containing 1 M $LiPF_6$ with a current rate of 0.2 C. b) CV profile at a scan rate of 0.01 mV s^{-1} using 1 M $LiPF_6$ in DMF as electrolyte. c,d) RDE measurements of ferrocene and ferrocenium in DMF containing 1 M $LiPF_6$ at various rotation rates ranging from 100 rpm to 4900 rpm at a scan rate of 5 mV s^{-1} on a glassy carbon electrode. e) Levich plot of limiting current (J_{lim}) vs. square root of rotation ($\omega^{1/2}$) of ferrocene and ferrocenium. f) Tafel plot derived from the rotation rate of 4900 rpm in the overpotential (η) range of 0.05 to 0.27 mV for ferrocene and ferrocenium.

ferrocene/ferrocenium redox reaction and DMF as solvent in the measured potential range. Increasing the sweeping rate led to a linear response of peak current density and square root of sweeping rate (SI, Figure S1), indicating the redox electrochemical process in the system was controlled by diffusion.

To gain further insight into the redox kinetics, rotation disk electrode (RDE) measurements were carried out to determine the diffusion coefficient of ferrocene/ferrocenium and the kinetic rate constant of the redox reaction. RDE measurements at a variety of rates yield the mass-transport-limited currents (Figure 2c,d). The Levich plot (Figure 2e) of the limiting current densities (J_{lim}) showed a linear response to the square root of rotation rates ($\omega^{1/2}$), from which the diffusion coefficient of ferrocene and ferrocenium could be determined to be 8.9×10^{-6} cm^2 s^{-1} and 3.2×10^{-6} cm^2 s^{-1}, respectively, based on the Levich equation [$J_{lim}=0.620\times nFD^{2/3}\omega^{1/2}\nu^{-1/6}C$, in which n is the number of electrons in the charge-transfer step, F is the faraday constant, ν is the kinematic viscosity ($\sim9.7\times10^{-3}$ cm^2 s^{-1}), and C is the prepared bulk concentration of the reactants (8×10^{-4} mol cm^{-3})]. The diffusion coefficient of ferrocene/ferrocenium in DMF is similar to those of redox couples in aqueous flow batteries,[23] but orders of magnitude higher than that in Li-ion batteries and NiMH batteries.[24,25] A Tafel plot of the kinetic current J_k showed a linear response to the overpotential (Figure 2f). Extrapolating the Tafel line to the equilibrium potential yields the exchange current density (J_0) of 1.05×10^{-3} A cm^{-2} and 5.13×10^{-4} A cm^{-2} for ferrocene and ferrocenium, respectively. The rate constant of the electron transfer, k_0, is proportional to the exchange current density according to $J_0=nFk_0C$ and results in the kinetic rate constant of 1.4×10^{-2} cm s^{-1} and 6.8×10^{-3} cm s^{-1} for ferrocene oxidation reaction and ferrocenium reduction reaction, respectively. Both values are greater than those found for other redox couples used in aqueous flow batteries such as VO_2^+/VO^{2+}, Fe^{3+}/Fe^{2+}, Ce^{4+}/Ce^{3+}, Cr^{3+}/Cr^{2+}, and Br^2/Br^-,[16] and are comparable to those of the I_3^-/I^- redox couple in aqueous phase.[26] This result implies that the voltage loss due to the rate of surface electrochemical reactions is negligible. The high rate can be attributed to an outer-sphere one-electron redox reaction with low energy barrier. Mass transfer of the electroactive species to the current collector surface is a major factor in determining the rate of an electrochemical oxidation or reduction, which can be further improved by an advanced current collector design that shortens diffusion pathways of electroactive materials.[27]

The Li^+ solid electrolyte membrane, often the bottleneck of mass transfer, did not restrain a high power output of the cell. Polarization-curve analysis showed that a maximum power output of 155 W kg^{-1} with a corresponding discharge potential of approximately 2.4 V could be achieved at room temperature based on the total weight of the ferrocene solution (Figure 3a). The cell could work shortly with the maximum power output in order to avoid possible Ti^{IV} reduction in the Li-ion conducting membrane when the voltage was below 2.8 V. The cell was able to deliver a rated power output of 120 W kg^{-1} with a current density of

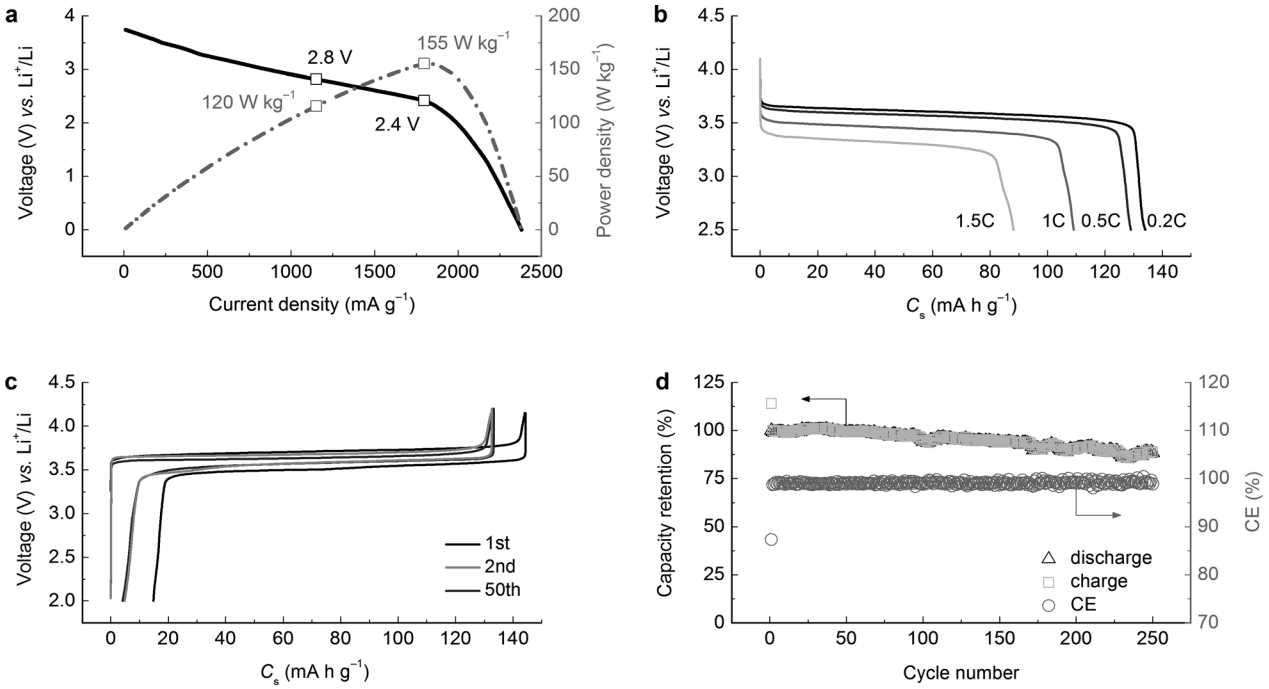

Figure 3. Electrochemical performance of the cell. a) Polarization curve and corresponding power density at room temperature. b) Room temperature cell discharge behavior at various C-rates of 0.2, 0.5, 1, and 1.5. The cell is fully charged to 4.15 V (vs. Li^+/Li) with a fixed C-rate of 0.2 prior to rate capability test. c) Representative charge/discharge profiles of the first, second, and 50th cycles. d) Capacity retention with corresponding Coulombic efficiency (CE) at room temperature over cycling.

1150 $mA\,g^{-1}$ (equals to C-rate of ~8). This power density is comparable to/exceeding that of the current battery technologies.[28] Increasing the conductivity of the Li-ion conducting membrane would significantly improve the power performance. For instance, the cell showed the rated power output of 165 and 210 $W\,kg^{-1}$ at elevated temperatures of 40 and 55 °C, respectively (SI, Figure S2). The capacity retention at different current densities (Figure 3b) showed that the cell reached a reversible capacity of 134 $mA\,h^{-1}\,g^{-1}$ with a discharge potential of ca. 3.6 V and a current density of 0.2 C, 94% of the theoretical capacity of ferrocene. Ohmic polarization resulted from the resistance of the Li-ion-conducting membrane and concentration polarization resulted from limited Li-ion transport in the solid electrolyte and ferrocenium diluent in the electrolyte became more obvious as the current density increased. Nevertheless, reversible capacities of 130, 110, and 90 $mA\,h^{-1}\,g^{-1}$ were delivered at higher current densities of 0.5, 1, and 1.5 C, respectively. It could be expected that the rate capability could be further enhanced with the development of superior Li^+-ion conductors,[29] which would benefit in promoting mass transfer between the anode and cathode. Galvanostatic charge/discharge measurements further demonstrated a stable cyclability of the cell. The initial charging capacity at a current density of 0.2 C reached 143 $mA\,h^{-1}\,g^{-1}$ (Figure 3c), almost the theoretical capacity of ferrocene (145 $mA\,h^{-1}\,g^{-1}$). A reversible capacity of around 130 $mA\,h^{-1}\,g^{-1}$ was achieved from the second cycle. An incomplete oxidation (~10%) of ferrocene was observed, which was caused by the diffusion-controlled electrochemical process. The potential was rather stable upon cycling and the average discharge potential reached 3.5 V. The overpotential was decreased from ca. 200 mV for the first cycle to ca. 150 mV at the second cycle, and further decreased to less than 100 mV at the 50th cycle, which is probably due to a gradually decreased interfacial resistance between the solution and the current collector.[7] The small overpotential resulted in a high energy efficiency of ca. 95% after the first cycle (SI, Figure S3), which is much greater than that of conventional redox-flow batteries (typically 65–75%).[30] The capacity retention was rather stable on cycling (Figure 3d), ca. 90% of the initial discharge capacity could be maintained after 250 full charge/discharge cycles with a capacity decay of ca. 0.4‰ per cycle. The Coulombic efficiency immediately reached 98% at the second cycle and stabilized between 98–100% thereafter.

The redox reaction of ferrocene and ferrocene-containing compounds shows high reversibility and electrochemical stability.[31] The solubility of the pristine ferrocene in organic solvents could be further increased by chemical functionalization of ferrocene, thus providing higher energy density.[32] The NMR analysis (SI, Figure S4) of the cells before and after cycling shows that the sharp peak resulting from the ferrocene ligand was not changed, indicating that the ligands of ferrocene are stable in the DMF-based electrolyte. The gradual capacity loss could be attributed to the anode, on which Li dendrites (SI, Figure S5) form upon cycling and detach from the current collector. Though the observed degradation of the LATP separator by Ti^{IV} reduction (when in direct contact with detached Li dendrite) is rather slow, as evident by the slightly increased cell resistance (SI, Figure S6), the LATP membrane does not show any structural deformation (SI, Figure S7). Compared with previous reports

using aqueous electrolytes,[3–6] DMF provides a wider potential range and alleviates the possible corrosion on the LATP membrane caused by H^+ or OH^- attack after long-term operation.[8,19] DMF as solvent in such a liquid cathode Li-redox battery avoids the use of a costly commercial organic electrolyte and can be operated in a broad temperature range owing to its relatively high boiling point (153 °C) and low freezing point (−61 °C).[33] The DMF solvent with its specific heat capacity (~140 $J K^{-1} mol^{-1}$) and thermal conductivity (~180 $mW K^{-1} m^{-1}$)[34] can effectively dissipate the heat, potentially offering an automatic cool-down system in case of a temperature increase or overloaded operation.[35] Nevertheless, it should be pointed out that the LATP separator, being the bottleneck of mass transfer, limited the cell to achieve higher power density. There's plenty of room to improve the conductivity of Li^+ conductors. For instance, a superionic Li^+ conductor based on $Li_{10}GeP_2S_{12}$ has recently been reported to exhibit a very high bulk conductivity of 12 $mS cm^{-1}$ at room temperature.[36]

In summary, the ferrocene/ferrocenium redox reaction in an aprotic solvent can be applied in a liquid cathode Li-ion redox battery for efficient electrical energy storage. The electroactive ferrocene/ferrocenium redox couple exhibits rapid redox kinetics with specific capacity over 130 $mA h^{-1} g^{-1}$. The redox reaction is highly reversible and efficient as the capacity maintains ca. 90% after 250 full charge/discharge cycles and the Coulombic efficiency reaches 98–100%. The cell shows a power density of 120 $W kg^{-1}$ based on the total weight of the liquid cathode, comparable to most current battery technologies. In addition, the liquid cathode is stable upon cycling and shows a mild reaction when short-circuited with metallic Li, thus making it a sustainable and safe energy storage medium. The ferrocene/ferrocenium redox couple has also been shown to work in a Na-ion battery with a semipermeable membrane.[9]

Received: June 12, 2014
Published online: August 27, 2014

Keywords: energy storage · ferrocene · Li-redox batteries · metallocenes · sustainable chemistry

[1] J. B. Goodenough, Y. Kim, *Chem. Mater.* **2010**, *22*, 587 – 603.
[2] B. Dunn, H. Kamath, J.-M. Tarascon, *Science* **2011**, *334*, 928 – 935.
[3] Y. Lu, J. B. Goodenough, Y. Kim, *J. Am. Chem. Soc.* **2011**, *133*, 5756 – 5759.
[4] N. F. Yan, G. R. Li, X. P. Gao, *J. Mater. Chem. A* **2013**, *1*, 7012 – 7015.
[5] Y. Zhao, L. Wang, H. R. Byon, *Nat. Commun.* **2013**, *4*, 1896.
[6] Y. Wang, Y. Wang, H. Zhou, *ChemSusChem* **2011**, *4*, 1087 – 1090.
[7] Y. Zhao, Y. Ding, J. Song, L. Peng, J. B. Goodenough, G. Yu, *Energy Environ. Sci.* **2014**, *7*, 1990 – 1995.
[8] T. Zhang, N. Imanishi, S. Hasegawa, A. Hirano, J. Xie, Y. Takeda, O. Yamamoto, N. Sammes, *J. Electrochem. Soc.* **2008**, *155*, A965 – A969.
[9] K. Park, J. H. Cho, K. Shanmuganathan, J. Song, J. Peng, M. Gobet, S. Greenbaum, C. J. Ellison, J. B. Goodenough, *J. Power Sources* **2014**, *263*, 52 – 58.
[10] Y. Chen, S. A. Freunberger, Z. Peng, F. Bardé, P. G. Bruce, *J. Am. Chem. Soc.* **2012**, *134*, 7952 – 7957.
[11] V. S. Bryantsev, V. Giordani, W. Walker, J. Uddin, I. Lee, A. C. T. van Duin, G. V. Chase, D. Addison, *J. Phys. Chem. C* **2013**, *117*, 11977 – 11988.
[12] S. Fery-Forgues, B. Delavaux-Nicot, *J. Photochem. Photobiol. A* **2000**, *132*, 137 – 159.
[13] D. O. Cowan, C. L. Vanda, J. Park, F. Kaufman, *Acc. Chem. Res.* **1973**, *6*, 1 – 7.
[14] Y. Wang, E. I. Rogers, R. G. Compton, *J. Electroanal. Chem.* **2010**, *648*, 15 – 19.
[15] A. S. Baranski, K. Winkler, *J. Electroanal. Chem.* **1991**, *313*, 367 – 375.
[16] A. Z. Weber, M. M. Mench, J. P. Meyers, P. N. Ross, J. T. Gostick, Q. Liu, *J. Appl. Electrochem.* **2011**, *41*, 1137 – 1164.
[17] D. Xiang, G. Gao, H. Shao, H. Li, H.-L. Zhang, H.-Z. Yu, *J. Phys. Chem. C* **2010**, *114*, 617 – 621.
[18] G. Y. Adachi, N. Imanaka, H. Aono, *Adv. Mater.* **1996**, *8*, 127 – 135.
[19] F. Ding, W. Xu, Y. Shao, X. Chen, Z. Wang, F. Gao, X. Liu, J.-G. Zhang, *J. Power Sources* **2012**, *214*, 292 – 297.
[20] Y. Lu, J. B. Goodenough, *J. Mater. Chem.* **2011**, *21*, 10113 – 10117.
[21] Y. Zhao, H. R. Byon, *Adv. Energy Mater.* **2013**, *3*, 1630 – 1635.
[22] I. Noviandri, K. N. Brown, D. S. Fleming, P. T. Gulyas, P. A. Lay, A. F. Masters, L. Phillips, *J. Phys. Chem. B* **1999**, *103*, 6713 – 6722.
[23] A. A. Shah, M. J. Watt-Smith, F. C. Walsh, *Electrochim. Acta* **2008**, *53*, 8087 – 8100.
[24] M. D. Levi, D. Aurbach, *J. Phys. Chem. B* **1997**, *101*, 4641 – 4647.
[25] X. Zhao, L. Ma, *Int. J. Hydrogen Energy* **2009**, *34*, 4788 – 4796.
[26] Y. Zhao, N. B. Mercier, H. R. Byon, *ChemPlusChem* **2014**, DOI: 10.1002/cplu.201402038.
[27] Y. Zhao, M. Hong, N. B. Mercier, G. Yu, H. C. Choi, H. R. Byon, *Nano Lett.* **2014**, *14*, 1085 – 1092.
[28] J.-M. Tarascon, M. Armand, *Nature* **2001**, *414*, 359 – 367.
[29] P. Knauth, *Solid State Ionics* **2009**, *180*, 911 – 916.
[30] C. Ponce de León, A. Frías-Ferrer, J. González-García, F. C. Walsh, *J. Power Sources* **2006**, *160*, 716 – 732.
[31] Y. Liang, Z. Tao, J. Chen, *Adv. Energy Mater.* **2012**, *2*, 742 – 769.
[32] Z. Song, H. Zhou, *Energy Environ. Sci.* **2013**, *6*, 2280 – 2301.
[33] D. R. Lide, H. V. Kehiaian, *CRC Handbook of thermophysical and thermochemical data*, CRC, Boca Raton, **1994**.
[34] G. Cai, H. Zong, Q. Yu, R. Lin, *J. Chem. Eng. Data* **1993**, *38*, 332 – 335.
[35] X. Wang, Y. Hou, Y. Zhu, Y. Wu, R. Holze, *Sci. Rep.* **2013**, *3*, 1401.
[36] N. Kamaya, K. Homma, Y. Yamakawa, M. Hirayama, R. Kanno, M. Yonemura, T. Kamiyama, Y. Kato, S. Hama, K. Kawamoto, A. Mitsui, *Nat. Mater.* **2011**, *10*, 682 – 686.

